



# 1 I. INTRODUCTION

[LIX08], [OZD03]. Processing of the signal can exploit the features produced by the concentration of signal energy in two dimensions (time and frequency), instead of in one dimension (time or frequency) [BOA03], [LIY03]. Noise tends to spread out evenly over the time-frequency domain, whereas signals concentrate their energies within limited time intervals and frequency bands; therefore, the local SNR of a 'noisy' signal can be improved simply by using time-frequency analysis [XIA99]. In addition, the intercept receiver can increase its processing gain simply by implementing time-frequency signal analysis [GUL08].

Time-frequency representations are valuable for the visual interpretation of signal dynamics [RAN01]. An experienced operator can more easily detect a signal and extract the signal parameters by analyzing a time-frequency representation, vice a time representation, or a frequency representation [ANJ09].

One of the members of the time-frequency analysis techniques family is the Wigner-Ville Distribution (WVD). The WVD has several desirable mathematical properties: it is always real-valued, it preserves time and frequency shifts, and it satisfies marginal properties [QIA02]. The WVD is computed by correlating the signal with a time and frequency translated version of itself, making it bilinear. The WVD has the highest signal energy concentration in the time-frequency plane [WIL06]. By using the WVD, an intercept receiver can come close to having a processing gain near the LPI radar's matched filter processing gain [PAC09]. The WVD, however, contains cross term interference (1)

The WVD of a signal  $x(t)$  is given in equation (1) as: 
$$WVD_x(t, f) = \int_{-\infty}^{\infty} x(t + \tau) x^*(t - \tau) e^{-j2\pi f\tau} d\tau$$

or equivalently in equation (2) as: 
$$WVD_x(t, f) = \int_{-\infty}^{\infty} x(t + \tau) x^*(t - \tau) e^{-j2\pi f\tau} d\tau$$

A lack of readability must be overcome to obtain time-frequency distributions that can be easily read by operators and easily included in a signal processing application [BOA03].

Some efforts have been made recently in that direction, and in particular, a general methodology referred to as reassignment.

The original idea of reassignment was introduced to improve the Spectrogram [OZD03]. As with any other bilinear energy distribution, the Spectrogram is faced with an unavoidable trade-off between the reduction of misleading interference terms and a sharp localization of the signal components.

We can define the Spectrogram as a twodimensional convolution of the WVD of the signal by the WVD of the analysis window, as in equation (3): 
$$S(t, f) = \int_{-\infty}^{\infty} \int_{-\infty}^{\infty} WVD_x(t, f) WVD_w(t', f') d t' d f'$$

Therefore, the distribution reduces the interference terms of the signal's WVD, but at the expense of time and frequency localization. However, a closer look at equation (3) shows that  $WVD_w(t', f')$  delimits a time-frequency domain at the vicinity of the  $(t', f')$  point, inside which a weighted average of the signal's WVD values is performed. The key point of the reassignment principle is that these values have no reason to be symmetrically distributed around  $(t', f')$ , which is the geometrical center of this domain. Therefore, their average should not be assigned at this point, but rather at the center of gravity of this domain, which is much more representative of the local energy distribution of the signal [AUG94]. Reasoning with a mechanical analogy, the local energy distribution  $WVD_x(t, f)$  (as a function of  $t, f$ ) can be considered as a mass distribution, and it is much more accurate to assign the total mass (i.e. the Spectrogram value) to the center of gravity of the domain rather than to its geometrical center. Another way to look at it is this: the total mass of an object is assigned to its geometrical center, an arbitrary point which except in the very specific case of a homogeneous distribution, has no reason to suit the actual distribution. A much more meaningful choice is to assign the total mass of an object, as well as the Spectrogram value, to the center of gravity of their respective distribution [BOA03]. This is precisely how the reassignment method proceeds: it moves each value of the Spectrogram computed at any point  $(t, f)$  to another point  $(t_r, f_r)$  which is the center of gravity of the signal energy distribution around  $(t, f)$  (see equations (4) and (5)) [LIX08]:

(5) 
$$t_r = \frac{\int_{-\infty}^{\infty} \int_{-\infty}^{\infty} t WVD_x(t, f) d t d f}{\int_{-\infty}^{\infty} \int_{-\infty}^{\infty} WVD_x(t, f) d t d f}$$

and thus, leads to a reassigned Spectrogram (equation (6)), whose value at any point  $(t, f)$  is the sum of all the Spectrogram values reassigned to this point: 
$$S_r(t, f) = \int_{-\infty}^{\infty} \int_{-\infty}^{\infty} S(t', f') \delta(t - t_r) \delta(f - f_r) d t' d f'$$

One of the most interesting properties of this new distribution is that it also uses the phase information of the STFT, and not only its squared modulus as in the Spectrogram. It uses this information from the phase spectrum to sharpen the amplitude estimates in time and frequency. This can be seen from the following expressions of the reassignment operators: Since time-frequency reassignment is not a bilinear operation, it does not permit a stable reconstruction of the signal. In addition, once the phase information has been used to reassign the amplitude coefficients, it is no longer available for use in reconstruction. For this reason, the reassignment method has received limited attention from engineers, and its greatest potential seems to be where reconstruction is not necessary, that is, where signal analysis is an end unto itself.

One of the most important properties of the reassignment method is that the application of the reassignment process to any distribution of Cohen's class theoretically yields perfectly localized distributions for chirp signals,

---

105 frequency tones, and impulses. This is one of the reasons that the reassignment method was chosen for this paper  
106 as a signal processing technique for analyzing LPI radar waveforms such as the triangular modulated FMCW  
107 waveforms (which can be viewed as back-to-back chirps).

108 To rectify the classical time-frequency analysis deficiency of cross-term interference, a method needs to be  
109 utilized that reduces cross-terms, which the reassignment method does.

110 The reassignment principle for the Spectrogram allows for a straight-forward extension of its use for other  
111 distributions as well [HIP00], including the WVD. If we consider the general expression of a distribution of the  
112 Cohen's class as a two-dimensional convolution of the WVD, as in equation (??1):(11)  $\rho(\omega, \delta \omega) \rho(\omega, \delta \omega)$ ;  
113  $= \int \rho(\omega - \omega', \delta \omega - \delta \omega') \rho(\omega', \delta \omega')$  (??, ??)????????? +? -?

114 replacing the particular smoothing kernel  $\rho(\omega, \delta \omega)$  by an arbitrary kernel  $\rho(\omega, \delta \omega)$  simply defines the  
115 reassignment of any member of Cohen's class (equations (??2) through (??4)): Now if we reverse our variables  
116 and look instead at the values of  $(\omega, \delta \omega)$  as a function of the image point coordinates  $(x, y)$ , then  
117  $\rho(\omega, \delta \omega) = \rho(\omega, \delta \omega) + \rho(\omega, \delta \omega)$  becomes  $\rho(\omega, \delta \omega) = \rho(\omega, \delta \omega) - \rho(\omega, \delta \omega)$  which also describes a straight line.(12) (14)  $\rho(\omega, \delta \omega)$ ;  
118  $\delta \omega = \rho(\omega, \delta \omega) - \rho(\omega, \delta \omega)$  (??, ??)????????? +? -? ?  $\rho(\omega, \delta \omega) - \rho(\omega, \delta \omega)$  (??, ??)  
119  $\rho(\omega, \delta \omega) + \rho(\omega, \delta \omega) - \rho(\omega, \delta \omega) = \rho(\omega, \delta \omega) - \rho(\omega, \delta \omega)$  (??, ??)????????? +? -?  
120  $\rho(\omega, \delta \omega) - \rho(\omega, \delta \omega) - \rho(\omega, \delta \omega)$  (??, ??)????????? +? -? ?? ?? (??) (??, ??)  $\rho(\omega, \delta \omega)$  ? ; ?) = ? ?? ?? +? -?

121 Consider two points  $\rho_1$  and  $\rho_2$ , which lie on the same line in the  $(\omega, \delta \omega)$  space. For each point, we can  
122 represent all possible lines through it by a single line in the  $(\omega, \delta \omega)$  space. Therefore, a line in the  $(\omega, \delta \omega)$  space  
123 that passes through both points must lie on the intersection of the two lines in the  $(\omega, \delta \omega)$  space representing  
124 the two points. This means that all points which lie on the same line in the  $(\omega, \delta \omega)$  space are represented by  
125 lines which all pass through a single point in the  $(\omega, \delta \omega)$  space.

126 To avoid the problem of infinite  $\rho$  values which occurs when vertical lines exist in the image, an alternative  
127 formulation,  $\rho = \rho \cos \theta + \rho \sin \theta$  (the parametric representation of a line) can be used to describe a line  
128 [CAR94], [DAH08]. This means that a point in the  $(\omega, \delta \omega)$  space (image space) is now represented by a sinusoid  
129 in  $(\rho, \theta)$  space (parameter space) rather than by a straight line. Points lying on the same line in the  $(\omega, \delta \omega)$   
130 space define sinusoids in the parameter space which all intersect at the same point. The more points that exist  
131 on that particular line in image space; the more sinusoids will intercept at that particular point in parameter  
132 space, and consequently, the more the accumulator value at this point (parameter space) will increase, forming  
133 a 'spike' in the parameter space. Therefore, 'spikes' (peak values) in the parameter space correspond to lines in  
134 the image space. The coordinates of the point of intersection of the sinusoids in the parameter space define the  
135 parameters of the line in the  $(\omega, \delta \omega)$  space (image space). For example, if we apply the Hough transform to  
136 the WVD of a chirp (line), we obtain a peak in the parameter space located in a position which depends on the  
137 parameter values (such as chirp rate) of the chirp (line) in the image space (the WVD plot) [SHA07] [XUL93].

138 This can best be shown by Figure ?? below: Figure ??: Time-frequency plot on the left and Hough transform  
139 plot on the right. A point in the TF plot maps to a sinusoidal curve in the HT plot. A line (signal) in the TF plot  
140 maps to a point in the HT plot. The rho and theta values of the point in the HT plot can be used to back-map  
141 to the TF plot, in order to find the location of the line (signal) (good if time-frequency plot is cluttered with  
142 noise and/or cross-term interference and signal is not visible)

143 In Figure ??, the image space (time-frequency plot) is on the left and the parameter space (twodimensional  
144 Hough transform plot) is on the right. Each point in the image space maps to a sinusoidal curve in the parameter  
145 space. The points 1, 2, and 3 in the image space map to the sinusoidal curves 1, 2, and 3 in the parameter space.  
146 In the parameter space, the intersection of the sinusoidal curves 1, 2, 3 at the point rho (x), theta (x) corresponds  
147 to the line connecting the points 1, 2, and 3 in the image space (same rho (x) and theta(x) values) [ISI96]. The  
148 more sinusoidal curves in the parameter space that pass through a particular point, the higher the accumulator  
149 value of that point will be and the higher the three-dimensional Hough Transform 'spike' will be [OLM01].  
150 The presence of a peak in the parameter space reveals the presence of Where  $\rho$  is the Dirac delta function.  
151 With  $\delta \omega = \rho \cos \theta + \rho \sin \theta$  (as noted in the figure above), each point  $(\omega, \delta \omega)$  in the original image  $\delta \omega$  is  
152 transformed into a sinusoid  $\rho = \rho \cos \theta + \rho \sin \theta$ , where, in the image,  $\rho$  is the perpendicular distance  
153 from the center of the image to the line at an angle  $\theta$  from the vertical axis passing through the center of the  
154 image. Again, points that lie on the same line in the image will produce sinusoids that all cross at a single point  
155 in the Hough plot.

156 The expression above gives the projection (line integral) of  $\delta \omega$  along an arbitrary line in the  
157 x-y plane. By definition, the Hough Transform computes the integration of the values of an image over all its  
158 lines.

159 From the signal location (rho and theta values) of the Hough transform plot, it is possible to back-map back  
160 to the signal location in the time-frequency representation, using the same exact rho and theta values.

161 Let's give an example of back-mapping, starting with the Hough Transform plot in Figure 2: The ability of the  
162 Hough Transform to perform well in low SNR environments, as well as in heavy crossterm environments makes it  
163 an ideal signal analysis tool to offset the classical time-frequency analysis deficiencies of cross-term interference  
164 and mediocre performance in low SNR environments. This makes for better readability, leading to more accurate  
165 parameter extractions for the intercept receiver signal analyst.

166 The joint sequential use of the RSPWVD and the Hough Transform (HT) will be used in this paper.

## 2 II. Methodology

The methodologies detailed in this section describe the processes involved in obtaining and comparing metrics between the joint sequential use of the Reassigned Smoothed Pseudo Wigner-Ville Distribution and the Hough Transform vs. the Reassigned Smoothed Pseudo Wigner-Ville Distribution signal processing techniques for the detection and characterization of low probability of intercept triangular modulated FMCW radar signals.

The tools used for this testing were: MATLAB (version 8.3), Signal Processing Toolbox (version 6.21), and Time-Frequency Toolbox (version 1.0) (<http://tftb.nongnu.org/>).

All testing was accomplished on a desktop computer (Dell Precision T1700; Processor -Intel Xeon CPU E3-1226 v3 3.30GHz; RAM -32.0GB; System type -64-bit operating system, x64-based processor).

Testing was performed for the triangular modulated FMCW waveform, whose parameters were chosen for academic validation of signal processing techniques. Due to computer processing resources they were not meant to represent real-world values. The number of samples was chosen to be 512, which seemed to be optimum size for the desktop computer. Testing was performed at three different SNR levels: 10dB, 0dB, and the lowest SNR at which the signal could be detected. The noise added was white Gaussian noise, which best reflects the thermal noise present in the IF section of an intercept receiver [PAC09]. Kaiser windowing was used, where windowing was applicable. 100 runs were performed for each test, for statistical purposes. The plots included in this paper were done at a threshold of 5% of the maximum intensity and were linear scale (not dB) of analytic (complex) signals; the color bar represented intensity. The signal processing techniques used for each task were the joint sequential use of the Reassigned Smoothed Pseudo Wigner-Ville Distribution and the Hough Transform vs. the Reassigned Smoothed Pseudo Wigner-Ville Distribution.

The triangular modulated FMCW signal (most prevalent LPI radar waveform [LIA09]) used had the following parameters: sampling frequency=4KHz; carrier frequency=1KHz; modulation bandwidth= 500Hz; modulation period=.02sec.

After each individual run for each individual test, metrics were extracted from the time-frequency representation. The metrics that were extracted were as follows:

1) Percent Detection: Percent of time signal was detected -signal was declared a detection if any portion of each of the signal components (4 chirp components for triangular modulated FMCW) exceeded a set threshold (a certain percentage of the maximum intensity of the time-frequency representation).

Threshold percentages were determined based on visual detections of low SNR signals (lowest SNR at which the signal could be visually detected in the timefrequency representation) (see Figure ??).

Figure ??: Threshold percentage determination. This plot is a time vs. amplitude (x-z view) of a signal processing technique of a triangular modulated FMCW signal (512 samples, with SNR=-3dB). For visually detected low SNR plots (like this one), the percent of max intensity for the peak z-value of each of the signal components (the 2 legs for each of the 2 triangles of the triangular modulated FMCW) was noted (here 61%, 91%, 98%, 61%), and the lowest of these 4 values was recorded (61%). Ten test runs were performed for this waveform for each of the signal processing techniques that were used. The average of these recorded low values was determined and then assigned as the threshold for that particular signal processing technique Based on the above methodology, thresholds were assigned as follows for the signal processing techniques used for this paper: RSPWVD + HT (60%); RSPWVD (60%).

For percent detection determination, these threshold values were included for each of the signal processing technique algorithms so that the thresholds could be applied automatically during the plotting process. From the time-frequency representation threshold plot, the signal was declared a detection if any portion of each of the signal components was visible (see Figure 5). The threshold percentage was determined based on manual measurement of the modulation bandwidth of the signal in the time-frequency representation. This was accomplished for ten test runs for each of the signal processing techniques that were used, for the triangular modulated FMCW waveform. During each manual measurement, the max intensity of the high and low measuring points was recorded. The average of the max intensity values for these test runs was 20%. This was adopted as the threshold value and is representative of what is obtained when performing manual measurements. This 20% threshold was also adapted for determining the modulation period and the time-frequency localization (both are described below).

For modulation bandwidth determination, the 20% threshold value was included for each the signal processing technique algorithms so that the threshold could be applied automatically during the plotting process. From the threshold plot, the modulation bandwidth was manually measured (see Figure 6). For modulation period determination, the 20% threshold value was included for each of the signal processing technique algorithms so that the threshold could be applied automatically during the plotting process. From the threshold plot, the modulation period was manually measured (see Figure 7). For lowest detectable SNR determination, these threshold values were included for each of the signal processing technique algorithms so that the thresholds could be applied automatically during the plotting process. From the threshold plot, the signal was declared a detection if any portion of each of the signal components was visible. The lowest SNR level for which the signal was declared a detection is the lowest detectable SNR (see Figure 8). From this threshold plot, the signal was declared a (visual) detection because at least a portion of each of the 4 signal components (the 2 legs for each of the 2 triangles of the triangular modulated FMCW) was visible. Note that the signal portion for the two 61% max intensities are barely visible, because the threshold for this particular signal processing technique is 60%. For this case, any lower SNR than -3dB would have been a non-detect

---

230 The data from all 100 runs for each test was used to produce the actual, error, and percent error for each of  
231 the metrics listed above.

232 The metrics for the joint sequential use of the Reassigned Smoothed Pseudo Wigner-Ville Distribution and the  
233 Hough Transform, along with the metrics for the Reassigned Smoothed Pseudo Wigner-Ville Distribution were  
234 generated. By and large, the joint sequential use of the Reassigned Smoothed Pseudo Wigner-Ville Distribution  
235 and the Hough Transform (RSPWVD + HT) outperformed the Reassigned Smoothed Pseudo Wigner-Ville  
236 Distribution (RSPWVD), as will be shown in the results section.

### 237 3 III. Results

238 Table 1 presents the overall test metrics for the two signal processing techniques used for this testing (the  
239 joint sequential use of the Reassigned Smoothed Pseudo Wigner-Ville Distribution and the Hough Transform  
240 (RSPWVD + HT) versus the Reassigned Smoothed Pseudo Wigner-Ville Distribution (RSPWVD)). 1, RSPWVD  
241 + HT outperformed RSPWVD in average percent error chirp rate (10dB: 0.41% vs. 1.58%), (0dB: 0.51% vs.  
242 2.81%), and (-3dB: 0.68% vs. 5.74%). RSPWVD + HT outperformed RSPWVD in average percent detection  
243 (10dB: 100% vs. 100%), (0dB: 100% vs. 92.4%), and (-3dB: 72.8% vs. 8.21%). RSPWVD + HT outperformed  
244 RSPWVD in average lowest detectable SNR (-5.04dB vs. -3.02dB).

245 Figure 9 shows comparative plots of the RSPWVD (left) vs. the RSPWVD + HT (right) (triangular modulated  
246 FMCW signal) at SNRs of 10dB (top row), 0dB (middle row), and lowest detectable SNR (-3dB for RSPWVD  
247 and -5dB for RSPWVD + HT) (bottom row).

### 248 4 IV. Discussion

249 This section will elaborate on the results from the previous section.

250 From Table 1, RSPWVD + HT outperformed RSPWVD in average percent error chirp rate (10dB: 0.41%  
251 vs. 1.58%), (0dB: 0.51% vs. 2.81%), and (-3dB: 0.68% vs. 5.74%). RSPWVD + HT outperformed RSPWVD  
252 in average percent detection (10dB: 100% vs. 100%), (0dB: 100% vs. 92.4%), and (-3dB: 72.8% vs. 8.21%).  
253 RSPWVD + HT outperformed RSPWVD in average lowest detectable SNR (-5.04dB vs. -3.02dB).

254 In previous research it was shown that the reassignment method, with its squeezing and For the RSPWVD +  
255 HT combination, the squeezing quality of the reassignment method, combined with the integration carried out  
256 by the Hough transform, makes for 'tighter' signals (equals more accurate theta value extraction and therefore  
257 more accurate chirp rate extraction (than for the RSPWVD alone), as per the results in Table 1), and makes  
258 for 'higher' signals (equals detecting the signal at lower SNR values (than for the RSPWVD alone), as per the  
259 results in Table 1), and better percent detection (than for the RSPWVD alone) due to the signal being that much  
260 higher than the noise floor, as per the results in Table 1). Therefore the joint sequential use of the RSPWVD  
261 and the HT allows for more accurate signal detection and parameter extraction of LPI radar signals than the  
262 RSPWVD alone, making for a more informed, effective, and safer intercept receiver environment, potentially  
263 saving valuable equipment, intelligence, and lives.

### 264 5 V. Conclusions

265 Digital intercept receivers, whose main job is to detect and extract parameters from low probability of intercept  
266 radar signals, are currently moving away from Fourier-based analysis and towards classical timefrequency  
267 analysis techniques (such as the WVD), and other novel analysis techniques. Though classical timefrequency  
268 analysis techniques are an improvement over Fourier-based analysis techniques, classical timefrequency analysis  
269 techniques, in particular the WVD, suffer from cross-term interference, which can make the time-frequency  
270 representation hard to read, especially if the components are numerous or close to each other, and the more so  
271 in the presence of noise. This lack of readability may equate to less accurate signal detection and parameter  
272 extraction metrics, potentially placing the intercept receiver signal analyst's platform in harm's way.

273 In previous research it was shown that the reassignment method, with its squeezing and smoothing qualities,  
274 reduces cross-term interference of classical time-frequency distributions (i.e. WVD), and produces more localized  
275 ('tighter') signals than those of the classical time-frequency distributions, making for improved readability, and  
276 consequently the extraction of more accurate metrics than the classical time-frequency distributions [STE21].

277 The research in this paper demonstrated that through the joint sequential use of the RSPWVD and the  
278 Hough Transform, the squeezing quality of the reassignment method, combined with the integration carried out  
279 by the Hough transform, made for 'tighter' signals (equals more accurate theta value extraction and therefore  
280 more accurate chirp rate extraction (than for the RSPWVD alone), as per the results in Table 1), and made for  
281 'higher' signals (equals detecting the signal at lower SNR values (than for the RSPWVD alone), as per the results  
282 in Table 1), and better percent detection (than for the RSPWVD alone) due to the signal being that much higher  
283 than the noise floor, as per the results in Table 1). Therefore the joint sequential use of the RSPWVD and the  
284 Hough Transform allows for more accurate signal detection and parameter extraction of LPI radar signals than  
285 the RSPWVD alone, making for a more informed, effective, and safer intercept receiver environment, potentially  
286 saving valuable equipment, intelligence, and lives.

## 5 V. CONCLUSIONS

287 Future plans include continuing to analyze low probability of intercept radar waveforms (such as the frequency  
288 hopping and the triangular modulated FMCW), using additional novel signal processing techniques, and  
comparing their results with research that has been conducted.

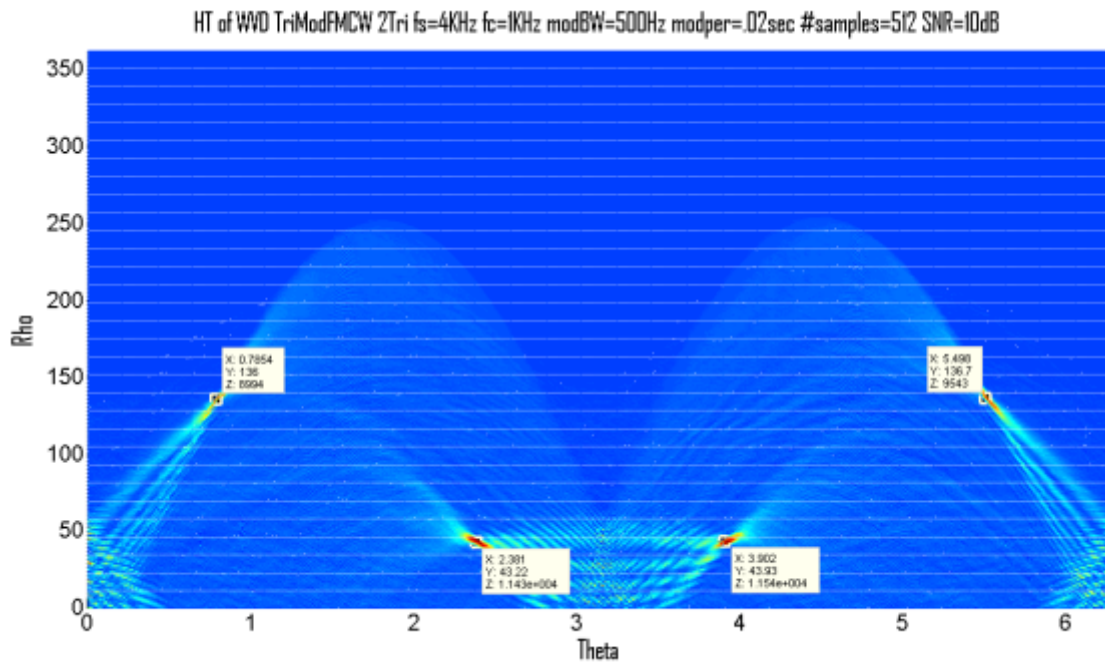


Figure 1: 3 ©

289

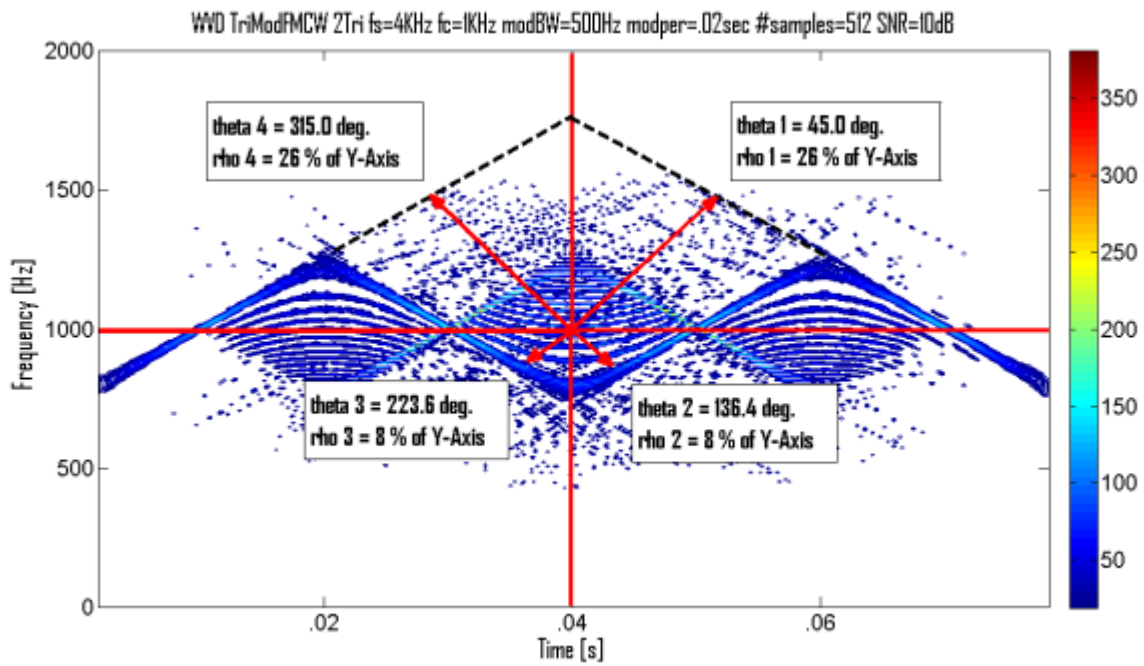


Figure 2:



Figure 3: Figure 2 :



Figure 4: Figure 3 :



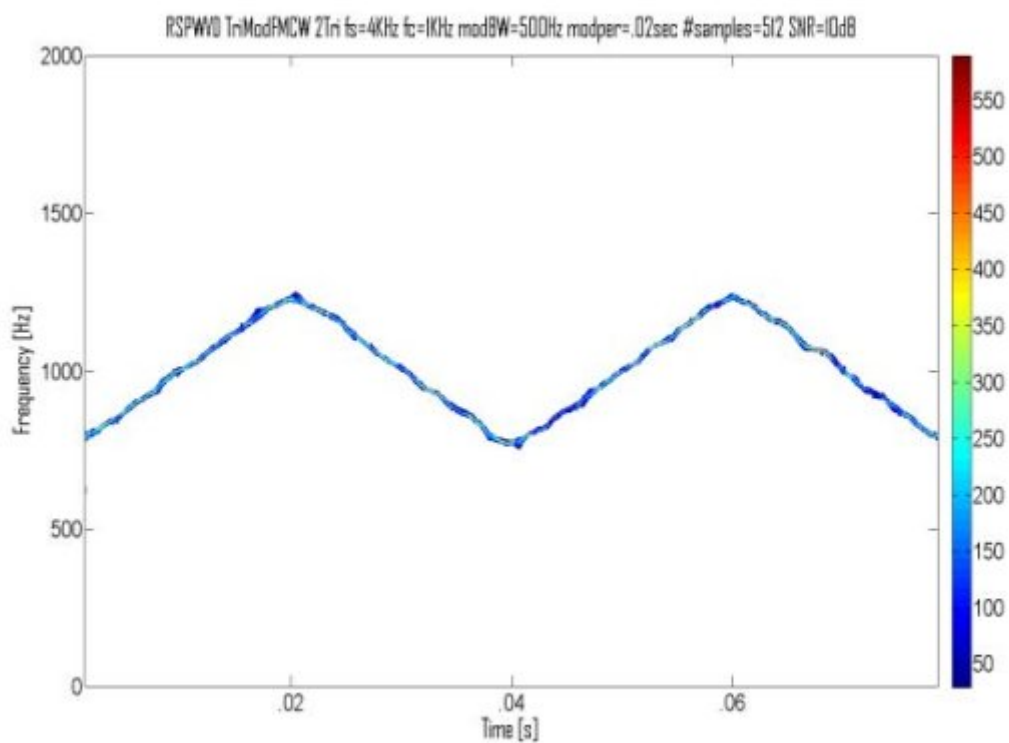
Figure 5: 7 ©



Figure 6: Figure 5 :

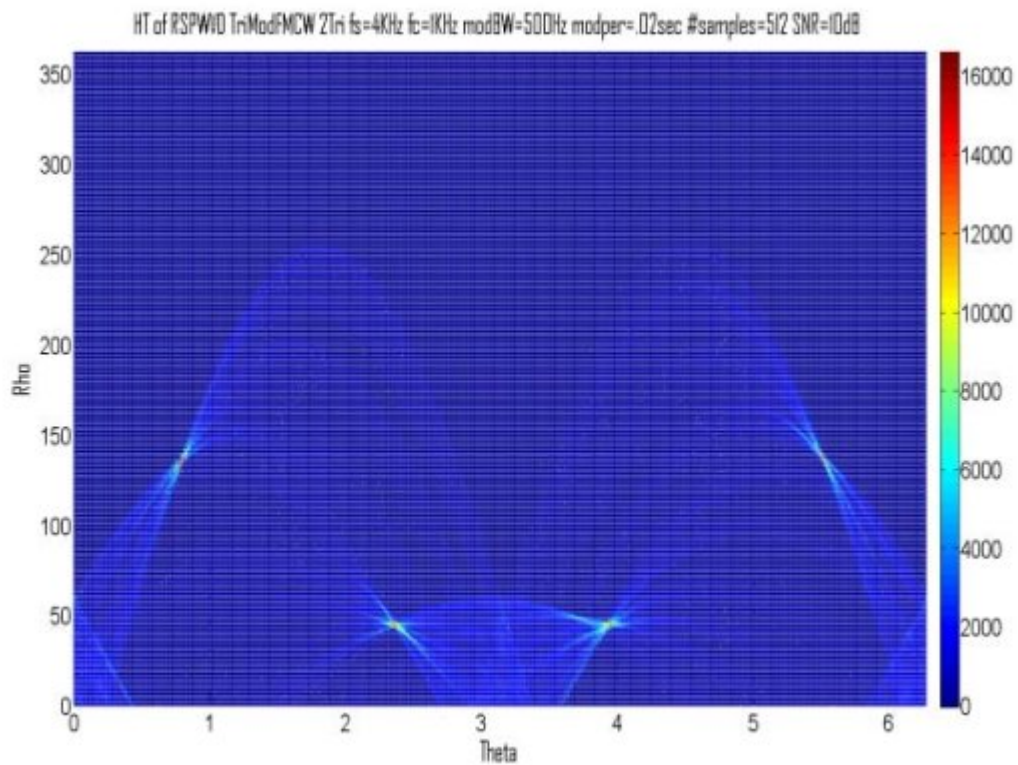


Figure 7: Global 8 ©



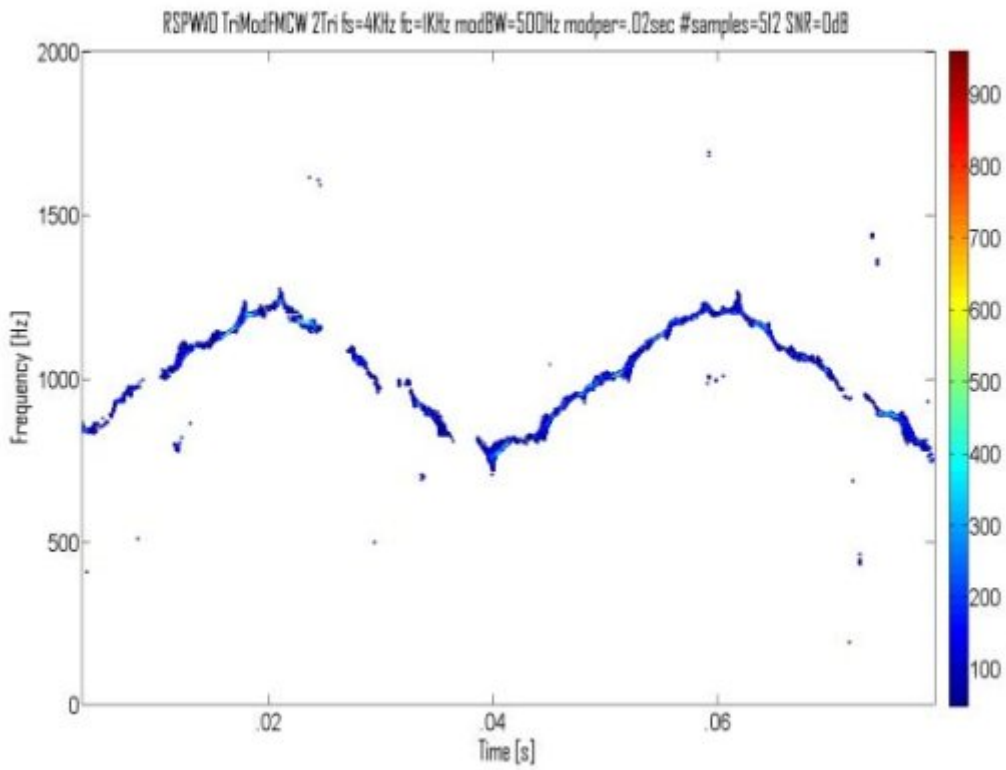
6

Figure 8: Figure 6 :



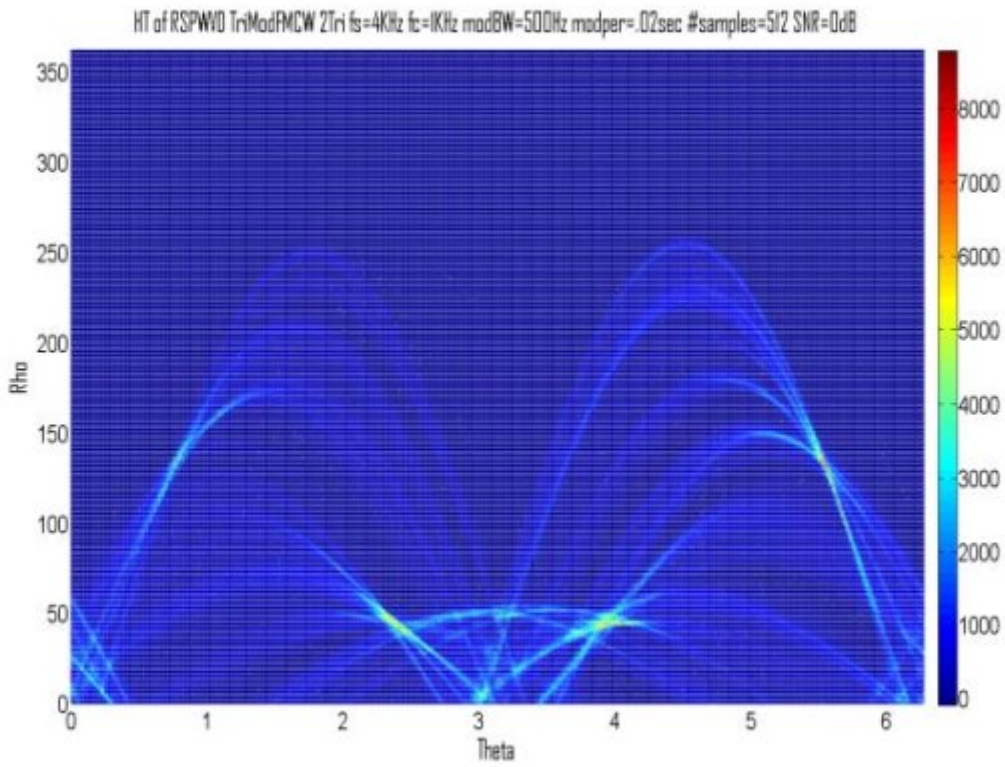
79

Figure 9: Figure 7 :Global 9 ©



8

Figure 10: Figure 8 :



9

Figure 11: Figure 9 :

Year 2023  
1  
© 2023 Global Journals

Figure 12: T

1

RSPWVD) -(chirp rate

Global Journal of Research in Engineering ( F ) XXIII Issue III Version I

Figure 13: Table 1 :

Year 2023  
11  
© 2023 Global Journals

Figure 14:

- 290 [Barbarossa and Zanalda ()] ‘A Combined Wigner-Ville and Hough Transform for Cross-Terms Suppression and  
291 Optimal Detection and Parameter Estimation’. S Barbarossa , A Zanalda . *ICASSP '92* 1992. 5 p. .
- 292 [Ste21] tevens (2021)]b33 ‘A Novel Approach for the Characterization of Triangular Modulated Frequency  
293 Modulated Continuous Wave Low Probability of Intercept Radar Signals via Application of the Wigner-  
294 Ville Distribution and the Reassigned Smoothed Pseudo Wigner-Ville Distribution’. D Ste21] Stevens . *Global  
295 Journal of Researches in Engineering: F, Electrical and Electronic Engineering* May 2021. 21 (2) p. .
- 296 [Anjaneyulu et al. (2009)] ‘A Novel Method for Recognition of Modulation Code of LPI Radar Signals’. L  
297 Anjaneyulu , N Murthy , N Sarma . ANJ09. *International Journal of Recent Trends in Engineering* May  
298 2009. 1 (3) p. .
- 299 [Xia ; Xia and Chen (1999)] ‘A Quantitative SNR Analysis for the Pseudo Wigner-Ville Distribution’. X Xia ;  
300 Xia , V Chen . *IEEE Transactions on Signal Processing* October, 1999. 47 (10) p. .
- 301 [Van Ginkel et al. ()] *A Short Introduction to the Radon and Hough Transforms and How They Relate to Each  
302 Other*, M Van Ginkel , C Luengo Hendriks , L Van Vliet . QI-2004-01. 2004. The Netherlands. Imaging Science  
303 and Technology Department, Delft University of Technology (Technical Report)
- 304 [Ste96] tephens (1996)]b34 ‘Advances in Signal Processing Technology for Electronic Warfare’. J Ste96] Stephens  
305 . *IEEE AES Systems Magazine* November 1996. p. .
- 306 [Olmo and Magli ()] ‘All-Integer Hough Transform: Performance Evaluation’. G Olmo , E Magli . OLM01. *IEEE  
307 Proceedings of the 2001 International Conference on Image Processing*, (Thessaloniki, Greece) October 7-10,  
308 2001. 13 p. .
- 309 [Zai99] aino and Bassett ()]b46 ‘An FPGA-Based Adaptive Computing Implementation of Chirp Signal  
310 Detection’. J Zai99] Zaino , R Bassett . RAAC 1999. p. .
- 311 [Barbarossa ()] ‘Analysis of Multicomponent LFM Signals by a Combined Wigner-Hough Transform’. S Bar-  
312 barossa . *IEEE Transactions on Signal Processing* 1995. 43 (6) p. .
- 313 [Auger et al. ()] F Auger , P Flandrin , P Goncalves , O Lemoine . ISI96. *Time-Frequency Toolbox Users Manual*,  
314 1996. Centre National de la Recherche Scientifique and Rice University
- 315 [Gulum ()] ‘Autonomous Non-Linear Classifications of LPI Radar Signal Modulations. Thesis, Naval Postgrad-  
316 uate School’. T Gulum . GUL07, (Monterey, CA) 2007.
- 317 [Boashash ()] B Boashash . BOA03. *Time Frequency Signal Analysis and Processing: A Comprehensive Reference*,  
318 (Oxford, England) 2003. Elsevier.
- 319 [Dahyot (2008)] R Dahyot . DAH08. *Bayesian Classification for the Statistical Hough Transform. International  
320 Conference on Pattern Recognition*, December 2008. p. .
- 321 [Pace ()] *Detecting and Classifying Low Probability of Intercept Radar*, P Pace . PAC09. 2009. Norwood, MA:  
322 Artech House.
- 323 [Pap ; Papandreou et al. ()] ‘Detection and Estimation of Generalized Chirps Using Time-Frequency Represent-  
324 tations’. A Pap ; Papandreou , G F Boudreaux-Bartels , S Kay . *Conference Record of the Twenty-Eighth  
325 Asilomar Conference on Signals, Systems and Computers*, 1994. 1994. p. .
- 326 [Hippenstiel et al. (2000)] ‘Detection and Parameter Estimation of Chirped Radar Signals’. R Hippenstiel , M  
327 Fargues , I Moraitakis , C Williams . HIP00. *Final Report* Jan. 10, 2000. Monterey, CA. Naval Postgraduate  
328 School
- 329 [Wang and Jiang ()] ‘Detection and Parameter Estimation of Multicomponent LFM Signal Based on the Cubic  
330 Phase Function’. Y Wang , Y Jiang . ID 743985. *EURASIP Journal on Advances in Signal Processing* 2008.  
331 2008. p. .
- 332 [Wong et al. (2009)] *Detection of Low Probability of Intercept Radar Signals*, K Wong , T Davidson , S Abelkader  
333 . 2009-142. September 2009. (Defence R&D Canada -Ottawa Contract Report)
- 334 [Sharif and Abeysekera (2007)] ‘Efficient Wideband Sonar Parameter Estimation Using a Single Slice of Radon-  
335 Ambiguity Transform’. R Sharif , S Abeysekera . SHA07, April 2007. 43 p. .
- 336 [Wil06] iley ()]b41 *ELINT: The Interception and Analysis of Radar Signals*, R Wil06] Wiley . 2006. Norwood,  
337 MA: Artech House.
- 338 [Gulum et al. (2008)] ‘Extraction of Polyphase Radar Modulation Parameters Using a Wigner-Ville Distribution-  
339 Radon Transform’. T Gulum , P Pace , R Cristi . GUL08. *IEEE International Conference on Acoustics, Speech,  
340 and Signal Processing*, (Las Vegas, NV) April 2008.
- 341 [Liw08] i et al. ()]b20 ‘Fast Estimation Method and Performance Analysis of Frequency Modulation Rate Via  
342 RAT’. W Liw08] Li , M Dan , X Wang , D Li , G Wang . *Proceedings of the 2008 IEEE International  
343 Conference on Information and Automation*, (the 2008 IEEE International Conference on Information and  
344 AutomationZhangjiajie, China) June 20-23, 2008. p. .

## 5 V. CONCLUSIONS

---

- 345 [Toennies et al. ()] *Feasibility of Hough Transform based Iris Localisation for Real-Time Application*, K Toennies  
346 , F Behrens , M Aurnhammer . TOE02. 2002. 02 p. .
- 347 [Rangayyan and Krishnan ()] ‘Feature Identification in the Time-Frequency Plane by Using the Hough-Radon  
348 Transform’. R Rangayyan , S Krishnan . *Pattern Recognition* 2001. 34 p. . (RAN01)
- 349 [Lia09] iang et al. ()]b19 ‘High-Speed Ground Moving Target Detection Research Using Triangular Modulation  
350 FMCW’. Y Lia09] Liang , L Zhang , M Xing , Z Bao . *Front. Electr. Electron. Eng* 2009. China. 4 (2) p. .
- 351 [Auger and Flandrin ()] ‘Improving the Readability of Time-Frequency and Time-Scale Representations by the  
352 Reassignment Method’. F Auger , P Flandrin . *IEEE Transactions on Signal Processing* AUG95. 1995. 43 (5)  
353 p. .
- 354 [Wang et al. ()] ‘Integrated Cubic Phase Function for Linear FM Signal Analysis’. P Wang , H Li , I Djurovic ,  
355 B Himed . *IEEE Transactions on Aerospace and Electronic Systems* 2010. (10) . (to appear)
- 356 [Lix08] i and Bi ()]b21 X Lix08] Li , G Bi . *A New Reassigned Time-Frequency Representation. 16 th European*  
357 *Signal Processing Conference*, (Lausanne, Switzerland) August 25-29, 2008. p. .
- 358 [Hough (1962)] ‘Method and Means for Recognizing Complex Patterns’. P V C Hough . HOU62. *U.S. Patent*  
359 December 18, 1962. 3 p. 69.
- 360 [Mil02] ilne and Pace]b23 P Mil02] Milne , P Pace . *Wigner Distribution Detection and Analysis of FMCW and*  
361 *P*, p. 4.
- 362 [Carranza et al. ()] ‘Motion Estimation by the Pseudo-Wigner Ville Distribution and the Hough Transform’. N  
363 Carranza , F Sroubek , G Cristobal . CAR06. *14 th European Signal Processing Conference*, (Florence, Italy)  
364 2006. p. .
- 365 [Nikolaev et al. ()] D Nikolaev , I Nikolaev , S Karpenko , P Nikolayev . NIK08. *Hough Transform: Underesti-*  
366 *mated Tool in the Computer Vision Field. 22 nd European Conference on Modeling and Simulation*, (Nicosia,  
367 Cyprus) June 3-6, 2008.
- 368 [Yasotharan and Thayaparan (2006)] ‘Optimum Time-Frequency Distribution for Detecting a Discrete-Time  
369 Chirp Signal in Noise’. A Yasotharan , T Thayaparan . *IEE Proc.-Vis. Image Signal Process*, April 2006.  
370 153 p. .
- 371 [Incer and Kaminsky ()] ‘Performance of Chirp-Slope Keying with Joint Time-Frequency Detectors’. I Incer , E  
372 Kaminsky . INC07. *Proc. of SPIE*, (of SPIE) 2007. OH. 6577 p. .
- 373 [Polyphase and Waveforms ()] Lpi Polyphase , Waveforms . *Proceedings of ICASSP*, (ICASSP Orlando, FL) 2002.  
374 p. .
- 375 [Qian ()] S Qian . QIA02. *Introduction To Time-Frequency and Wavelet Transforms*, (Upper River, NJ) 2002.  
376 Prentice Hall.
- 377 [Xu and Oja (1993)] ‘Randomized Hough Transform (RHT): Basic Mechanisms, Algorithms, and Computational  
378 Complexities’. L Xu , E Oja . *XUL93*, March 1993. 57 p. .
- 379 [Liy03] i and Xiao (2003)]b22 ‘Recursive Filtering Radon-Ambiguity Transform Algorithm for Detecting Multi-  
380 LFM Signals’. Y Liy03] Li , X Xiao . *Journal of Electronics (China)* May 2003. 20 (3) p. .
- 381 [Carlson et al. (1994)] ‘Search Radar Detection and Track with the Hough Transform, Part I: System Concept’.  
382 B Carlson , E Evans , S Wilson . CAR94, January 1994. 30 p. .
- 383 [Han00] an et al. (2000)]b14 ‘Target Position Extraction Based on Instantaneous Frequency Estimation in a  
384 Fixed-Reticule Seeker’. S Han00] Han , H Hong , D Seo , J Choi . *Opt. Eng* September 2000. 39 p. .
- 385 [Thuc and Duc ()] ‘The Hough Transform -A Radon-Like Transform’. N Thuc , D Duc . *International Conference*  
386 *on Electronic Information*, 2004. 2004.
- 387 [Toronto et al. (2007)] ‘The Hough Transform’s Implicit Bayesian Foundation’. N Toronto , B Morse , D Ventura  
388 , K Seppi . IV-377 -IV-380. *IEEE International Conference on Image Processing*, October 2007. 4.
- 389 [Auger and Flandrin ()] ‘The Why and How of Time-Frequency Reassignment’. F Auger , P Flandrin . *IEEE*  
390 *International Symposium on Time-Frequency and Time-Scale Analysis*, AUG94. 1994. p. .
- 391 [Ozdemir (2003)] *Time-Frequency Component Analyzer*, A Ozdemir . OZD03. Sept. 2003. Ankara, Turkey.  
392 Bilkent University (Dissertation)
- 393 [Duda and Hart (1972)] ‘Use of the Hough Transformation to Detect Lines and Curves in Pictures’. R Duda , P  
394 Hart . DUD72. *Comm. ACM* January 1972. 15 (1) p. .
- 395 [Ben05] ennett and Saito ()]b5 *Using Edge Information in Time-Frequency Representations for Chirp Parameter*  
396 *Estimation. Applied Computational Harmonic Analysis*, N Ben05] Bennett , N Saito . 2005. p. .
- 397 [Wei03] ei et al. (2003)]b40 G Wei03] Wei , S Wu , E Mao . *Analysis of Multicomponent LFM Signals Using Time-*  
398 *Frequency and The Gray-Scale Inverse Hough Transform. IEEE Workshop on Statistical Signal Processing*,  
399 September 28 -October 1, 2003. p. .